Ilorin Journal of Science
Volume 7, Number 2, 2020, pp. 144 – 162 (Printed in Nigeria)
ISSN: 2408 – 4840 © 2020 Faculty of Physical Sciences, University of Ilorin
https://doi.org/10.54908/iljs.2020.07.02.002

ILORIN
JOURNAL OF SCEINCE

ILJS-20-009

Integrated Geological and Geophysical Data as an Aid to Surface Geological Mapping and Mineral Exploration of the Ibillo-Okene Area SouthWest Nigeria

Ajigo*, I. O., Ademeso, O. A. and Odeyemi, I. B.

Department of Applied Geology, Federal University of Technology, Akure, Ondo State, Nigeria.

Abstract

Ibillo-Okene area located at the northern fringe of the Igarra Schist belt, is a part of the Basement Complex rocks of southwest Nigeria. Aerogeophysical Datasets were used in conjunction with field data in order to interpret the geology and structure of this area. Five major lithological units were identified in the study area including migmatites, biotite schist, quartz schist, granite gneiss, and calc silicate gneiss which is associated with marble. Three episodes of deformation in the study area include that captured by relics of meta-pelitic (basic) rocks caught up (as xenoliths) in the main phase gneisses, that which produced the fabric in the main phase gneisses as well as metasedimentary rocks and that which is associated with Pan-African orogenic event which apparently modified the earlier two. Orientation of dominant foliation planes gives a general outline of the closure of the ancient basin; late-stage, brittle-ductile deformation resulted in the compression of this basin and subsequent faulting. This NW-SE trending fault reported in the present study area is an extension of a gold-bearing fault reported south, around Dagbala-Atte area. Also, metasedimentary rocks found here are associated with marble just like their counterpart in the southern parts of the Igarra schist belt.

Keyword: Migmatite, foliation, aerogeophysical data, Schist belt, fault.

1. Introduction

Airborne magnetic and radiometric surveys have been used extensively in the mineral exploration industry predominantly for the delineation of metalliferous deposits (Airo and Loukola-Ruskeeniemi, 2004; Patra *et al*., 2013; Wemegah *et al*., 2015). Its application ranges from mineral exploration (Murphy, 2007), structural mapping and rock characterization (Telford *et al*., 1990). Recent advances in technology have substantially increased the accuracy and resolution of these techniques so that they can be used to provide useful, enhanced information on lithology and geological structures. Additionally, advances in data analysis, processing and image enhancement techniques have improved the resolution of geophysical datasets further to the extent that very subtle variations in the geophysical

*Corresponding author: Ajigo, I. O.
Email address: ioajigo@futa.edu.ng

responses can be identified (Armstrong and Rodeghiero, 2006; Ansari and Alamdar, 2009; Dickson and Scott, 1997; Geosoft Inc. 1995 & 1996).

The physical principles of aeromagnetic methods are based on taking measurements of the ambient magnetic susceptibility of the surface geology and using the data to determine the distribution of magnetic minerals and hence changes in lithology (Reynolds *et al*., 1990; Telford *et al.*, 1990). Wilford *et al.* (1997) indicated that airborne radiometric survey is similarly used to measure variations in the radioactive mineral composition in order to map lateral lithological changes. This method involves the measurement of naturally occurring radioactive elements that exist in rock forming minerals and soil profiles. These elements are uranium (U), thorium (Th) and potassium (K), which can be found as trace elements in all rocks and decay naturally giving off gamma radiation or rays (Boadi *et al*., 2013; Minty, 1998; Minty and Hoygarrd, 2002; Wilford, 2002). The variation of magnetic and radiometric mineral composition in rocks due to the difference in lithological set up and mineralization processes such as hydrothermal mineralization make the use of these methods in mapping rock lithology, structures and mineral zones a useful technique (Richardson, 1983; Silva *et al*., 2003).

Odeyemi (1988) reported two limbs of regional fold in the southern part of the Igarra Schist Belt; this regional and other associated structures which have been found to have age as well as economic significance, is seen to have extended to and closed in the northern fringe of the belt, which is the present study area. Furthermore, a major fault with NNW-SSE trend was reported around Dagbala and Atte by Adepoju (2017) directly south of the present study area. Regional geological structures are better appreciated using remotely-sensed data which enable a more comprehensive interpretation when combined with field verification.

This paper discusses aeromagnetic and radiometric datasets from the Ibillo-Okene area of one of the metasedimentary belts of south-western Nigeria. This is to help map the geology and to delineate possible economic mineral-hosting, geological structure within this part of the belt. This research seeks to, in interpreting remotely-acquired data, delineate geology, regional and local geological structures (shear zones and faults) that have the potential of hosting mineralization within the study area. This work therefore aims at highlighting target areas for detailed exploration work in search for economic mineralization within the Ibillo-Okene axis which has not been extensively explored as compared to the southern parts of the Igarra metasedimentary (schist) belt, of which the present study area is a northern fringe.

2. Regional Geologic Setting and Mineralization

A large portion of West Africa sub-region, including the whole of Nigeria, carries the imprint of the Late-Proterozoic Pan-African Orogeny, whose effects are largely a reworking of older, polycyclic crust. This polycyclic crust has been given dates corresponding to the Liberian (2700 ± 200 Ma), Eburnian (2000 ± 200 Ma) and Kibaran (1100 ± 200 Ma) Orogenic events, (Turner, 1983). The Pan-African province of West Africa lies between two Cratons of Archaean to Lower Proterozoic age: the West African Craton to the west and the Congo Craton to the south-east (Fig. 1). Eastward, the Pan-African province probably continues across the whole width of Africa to link with the Mozambique Belt of East Africa. Northward, it extends through the Hogger massif in the Central Sahara to be truncated by the Alpine fold Belt of North Africa (Udinmwen *et al.*, 2016).

Seventeen main schist belts have so far been identified in Nigeria. The metavolcano-sedimentary sequences in these belts have been found to show a close similarity to those of the schist belts in other parts of the world which are known to host important precious metal (gold, silver, cadmium, etc.) and other mineral deposits (Annor *et al.*, 1996; Olobaniyi and Annor, 1997 etc.). In fact, there is local, traditional belief that gold not only occurs, but has also been mined in the Igarra schist belt especially around Dagbala (Adepoju, 2017; 1999).

The Igarra area, which is directly south of the present Ibillo-Okene study area, has been mapped by Odeyemi (1997, 1988 and 1990). In this area, migmatites, biotite- and biotite-hornblende gneisses occurred interbanded with low-grade metasediments consisting of schists, calc-silicate gneiss, marbles, polymict metaconglomerate and quartzites. Intrusions of syn- to late-tectonic older granites, charnockites and gabbros cut through the schists, gneisses and migmatites. Dykes of unmetamorphosed dolerite, pegmatite, aplite, lamprophyres and syenites are present in all the pre-existing rock groups. The low grade met sediments (Igarra schist belt) are the most dominant rock in this area. According to Hockey *et al*. (1986), east of the present study area, around Okene area, the geology comprises of steep-dipping gneisses and migmatites which give rise to knife-edge ridges. Bands of quartzite which occur both in the migmatite-gneiss complex and in the more schistose areas, form hog-back ridges, covered by rubbles of quartzite fragments. In areas underlain by metasediments, comparatively thin bands of quartzites (and even quartz-schists), form distinctive linear ridges because of their relatively higher resistance to weathering.

The geology of the present study area is thus dominated by the Nigerian Basement Complex rocks comprising of migmatites overlain by the North-South trending bands of metasedimentary schists (Fig. 2) as well as the metavolcanics. Migmatitic gneisses widens out very substantially north and southeast of the study area. Metasedimentary units of the Igarra Belt dominate the south, extending up to the southwest of Ibillo town. To the northwest, migmatitic gneisses dominate, from where they extend to part of the western part of the study area. A peculiar feature of the metasedimentary schist is the consistent association of calc-silicate gneiss/marble and metaconglomerate with the quartz and mica schist where they are seen to have been folded together (Odeyemi, 1988). Wright *et al*. (1985) also reported the occurrence of iron (magnetite and hematite) and manganese ores in association with metapellitic schist.

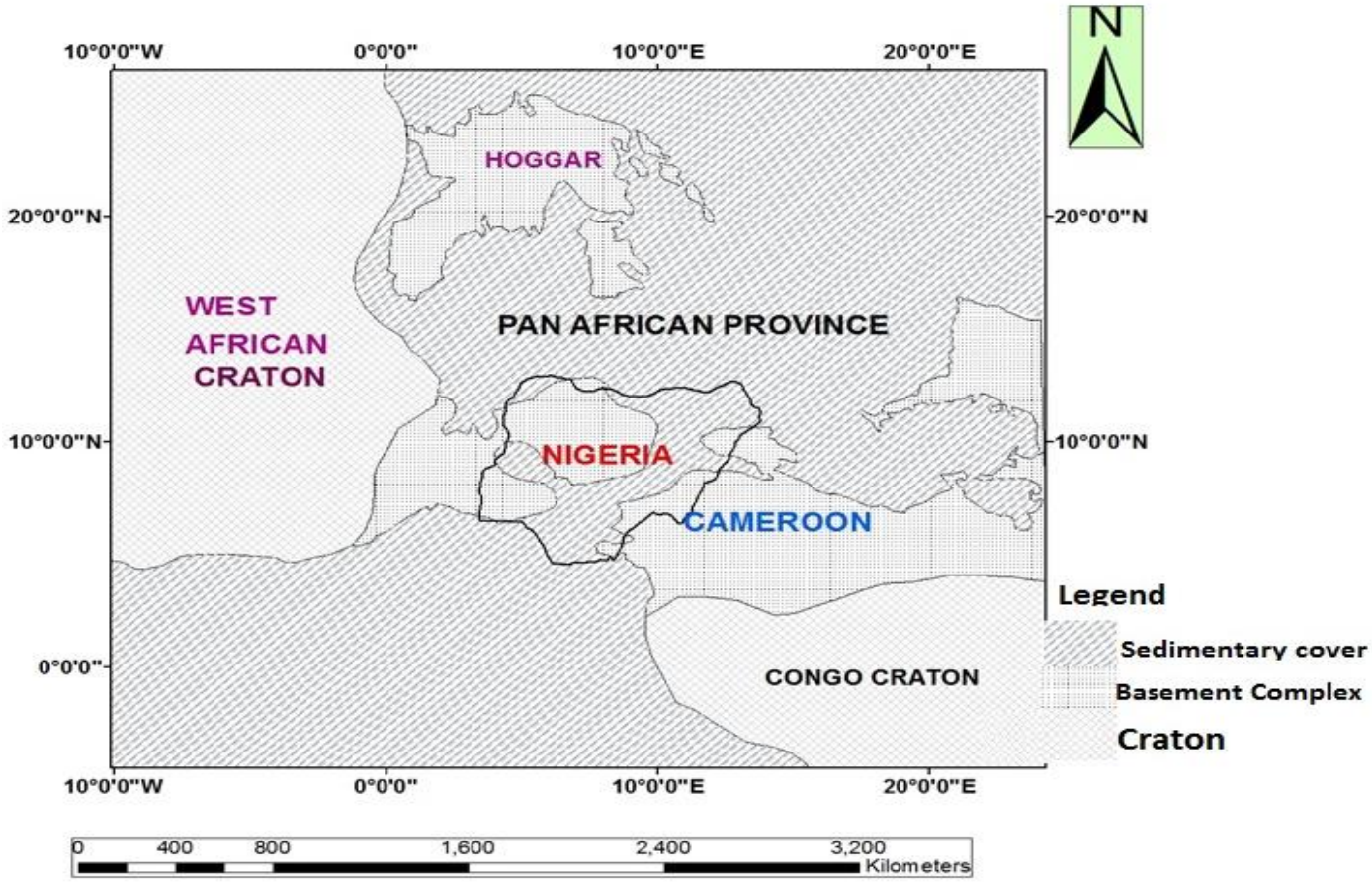

Figure 1: Nigeria within the Pan African Province. (Modified after Ajibade *et al.*, 1988).

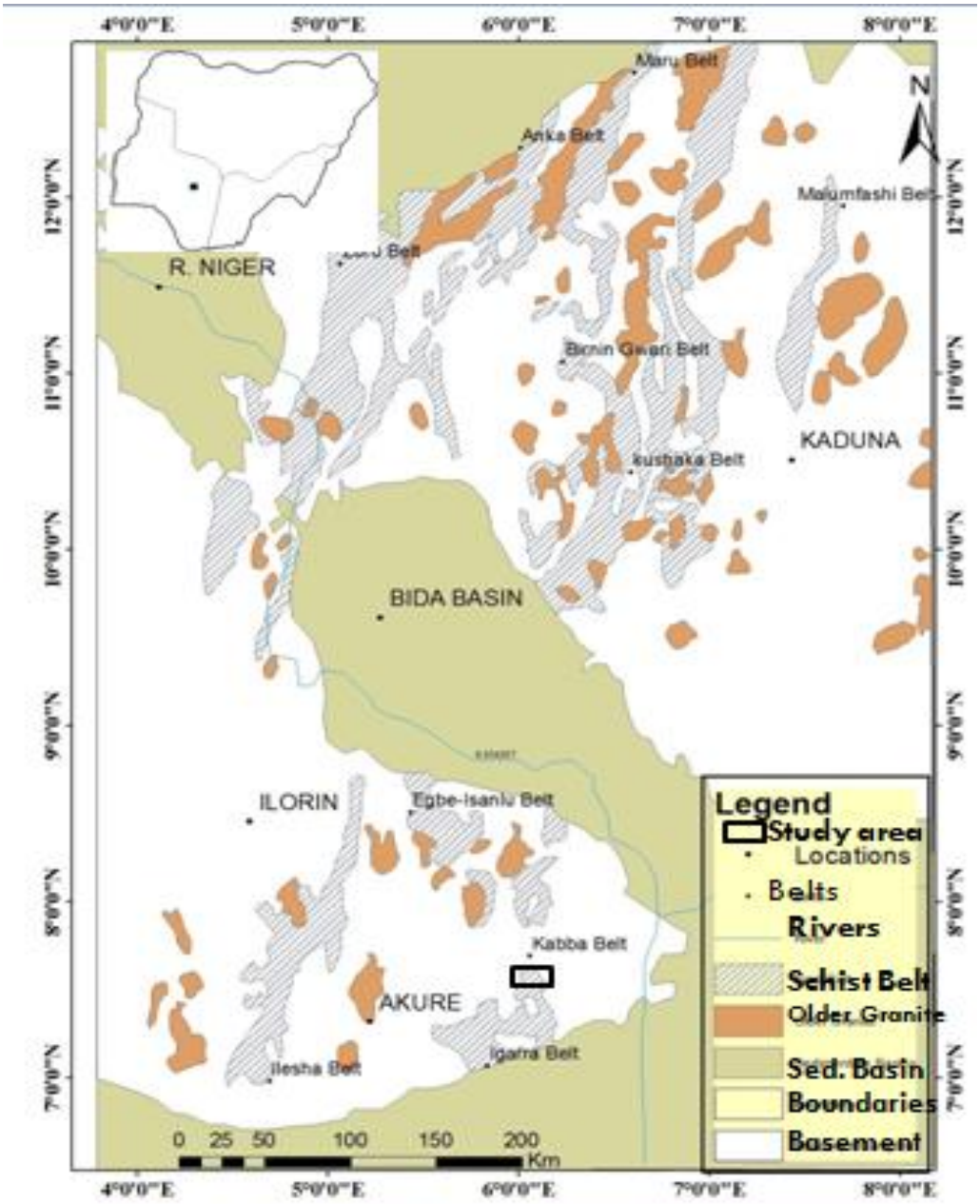

Figure 2: Geological map of part of Nigeria showing the location of the study area within the schist belts (After Muecke, 2005).

3. Materials and Methods

High resolution airborne geophysical data was sourced from the Nigerian Geological Survey Agency (NGSA), Abuja. The data which was collected systematically by dividing the country into geological blocks with dissimilar measurement parameters for each block resulted in the eventual production of aerogeophysical maps for the whole country with varying specifications (Table 1). Geophysical data for this study were procured from this data bank.

The study area cuts across two map sheets of Auchi sheet 266 (northwest segment) and Kabba sheet 246 (southwest segment).

Table 1: Airborne Geophysical survey parameters (MMSD, 2010).

Survey Parameter	**Parameter Specification**
Year	2004-2009
Travel line spacing	500 m
Travel line direction	NW-SE
Tie-line spacing	2km
Tie-line direction	NE-SW
Normal terrain clearance	80 m
Navigation	Global Positioning System (GPS)
Sampling time	0.1 s (magnetic), 1.0 s (radiometric)
Air speed (nominal)	250-290 km/h (70-80 m/s)
Measurement spacing	8 m (magnetic), 80 m (radiometric)

Total magnetic intensity map was subjected to series of processes such as reduction to equator and different types of filtering with a view to enhancing the interpretability of the images. Filtering includes Butterworth low pass, downward/upward continuation, tilt/vertical derivatives filters etc. The aim of these include elimination of noise or error in the data, enhancement of responses in the magnetic data among others. Similar processes were applied to radiometric data in addition to window stripping used to isolate count rates from the individual radionuclides K, U and Th. In order to correct for the much undulating topography in parts of the study area, (600–2040 m above sea level), correction both for variations in ground clearance and ground geometry using stripped window count rates method of Schwarz *et al.* (1992) was applied. Residual line-level errors (remaining inconsistencies between adjacent flight lines) were removed by passing a median filter over the data set, in accordance with the method of Mauring and Kihle (2006). Finally, radionuclide count rates were converted to ground element concentrations using calibration values. The processed data produced three maps: equivalent thorium concentration (eTh) in ppm, equivalent uranium concentration (eU) in ppm and potassium concentration in %.

Lineament statistics were generated and used to construct lineament density map, as well as Rose diagram to show the orientation of the regional trend of deformation. In order to establish the spatial density of the lineament, the lineament map was gridded into sub-grids, and the total length of all lineaments in each grid was estimated from the summation of the individual lineament lengths within each grid; the total length obtained was plotted at the centre of each grid. The coordinates of each grid together with the length/grid was then used to produce the lineament density map. Lastly, field data acquisition was carried out to validate and enhance the remotely-sensed data for informed interpretation and subsequent preparation of litho-structural map of the study area.

4. Results and Discussions

Remotely-sensed data of magnetic as well as radiometric data though not conclusive by themselves in geological investigation, prove useful as tools for interpretation of structures and lithological disposition subject to field verification. Furthermore, consistent orientations of the lineaments from these sources and their positive relationships with the underlying geologic units clearly suggest that they represent discontinuity in these rock units, a further confirmation of their reliability when properly applied.

4.1. Aeromagnetic Data

Derivatives of the total magnetic intensity (TMI) maps forms the basis for interpretations where change in magnetic response helped to deduce the subtle variation, occasioned by change in geology or structural disposition of the various units that make up the study area, are enhanced for proper interpretation. Areas of long stretch of low to medium magnetic susceptible pattern denoted as Ms_1, corresponds to the meta-sedimentary rocks and their remnants as thin soil layers (Figure 3a). The broad E-W high magnetic susceptible patterns $_{Mg1}$, Mg_2 and Mg_3 at the central-part of Figure 3a represent the migmatites. Unlike the radiometric data maps, the TMI map could not clearly indicate distinct boundary between the different meta-sedimentary units but differentiate broadly between these units (to the south of the study area) and the migmatites; the reason for this is attributed to relatively low magnetic minerals content of the metasediments. Analytical signal map further refined this differentiation into negative to low magnetic intensity area which is underlain by the metasedimentary units and a medium to high magnetic intensity area that is underlain by migmatite and other rocks. Analytical signal, total horizontal and tilt derivative maps show

the regional structural grain of a dominant NW-SE and a subordinate NE-SW depicting the closure of the metasedimentary basin.

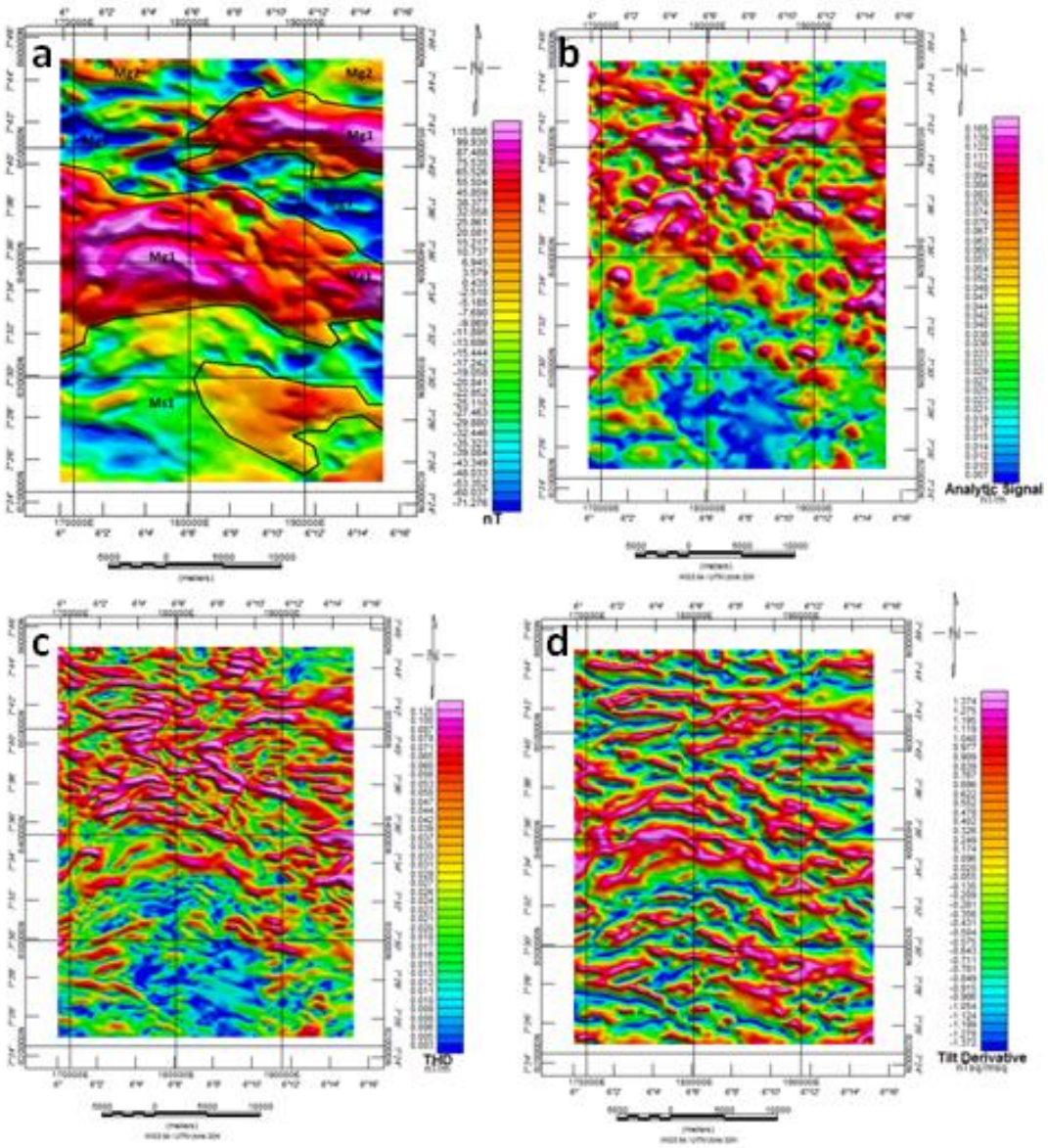

Figure 3: (a) Total magnetic intensity map (b) Analytical signal map (c) Total horizontal derivative map (d) Tilt derivative map of the study area.

4.2. Radiometric Data

The underlying principle of the use of potassium, thorium and uranium is based on the fact that the response of rocks depends on the level of enrichment/impoverishment with respect to these elements. Each of these elements have their own geochemically associated elements in definite geochemical environment, such that the presence/absence of one may influence same of geochemically associated elements. Furthermore, potassium and thorium are generally considered immobile in most geochemical environment. The processed airborne data show

that regions dominated by different rock types vary significantly in mean Uranium, thorium and potassium concentrations, although there are areas of slight overlap in terms of these concentrations.

Boadi *et al*. (2013) demonstrated that only a few decimetres of soil sediments are enough to effectively shield gamma radiation emitted by underlying thorium- and uranium-bearing rocks. Consistent with this, areas of superficial (soil) deposits derived from weathered metasedimentary units, which overlie the migmatite in some portions of this area are marked by low concentrations of radio-elements, (< 2 % eK, Figure 4a), (< 10 ppm eTh, Figure 4b) and uranium (< 2 ppm eU, Figure 4c) on Th and U maps. Uranium, Thorium and Potassium concentrations in the study area are in the range between 0.9 ppm – 5.4 ppm, 7.0 ppm – 30ppm and 0.6% - 3.9 % respectively. Observations revealed relatively high concentrations (up to 30 ppm eTh and 5.4 ppm eU) in areas where migmatite/gneiss complex and their weathered products are at or near the land surface around Ogori-Magongo-Okene axis, (figure 4).

At first glance, a first-order correlation between thorium and uranium concentrations on the one hand and potassium and thorium on the other seems to exist in parts of the study area underlain by the migmatites. However, thorium/uranium ratio varies significantly between the different rock types. Shives et al. 2000, observed that radiometric survey image with particularly strong anomaly are most often related to felsic minerals while low concentrations are related to mafic minerals**.** Obliteration of the rock surface in parts of the study area is interpreted to be responsible for the non-uniformity of radiometric signature across the area. Also, areas of relatively high concentration of potassium may be due to processes relating to hydrothermal alteration.

A generalized qualitative overview of radiometric maps revealed that, migmatitic gneisses in the eastern, western and extreme north-eastern parts of the study area are relatively high in potassium concentration. Those in the central and north-western parts are intermediate in potassium concentration while the metasediments and their weathered products are low in potassium concentration. Similarly, thorium concentration is highest on the areas with exposed migmatitic gneisses, intermediate in the metasedimentary units and low in areas covered with weathered materials constituting soil cover. Uranium on the other hand is intermediate/high in concentration across areas with both migmatite and metasediments and low in concentration in areas with weathered material cover.

The Ternary image (Figure 4d) comprises of colours generated from the relative intensities of the three components and represents subtle variations in the ratios of the three bands. Potassium was assigned to red, uranium to blue and thorium to green. Parts of the migmatite and quartz-rich sandy materials appeared darker than the surrounding units, indicating lower concentrations in K, U, and Th. The white areas in the ternary image are indication of high concentration of potassium, thorium and uranium resulting from felsic materials. The magenta shows areas of high K and U but low Th concentrations whilst the yellow indicates areas of high K and Th but low U concentrations.

The ternary map shows high thorium concentration in the north-west particularly around farm lands derived from weathered thin layer of metasedimentary units, while thicker, well exposed metasedimentary units at the central and south-western corner of the image record high U. The quartz schist, east of Lampese has its boundary delineated on the basis of constituent radiometric elements contrast. Another distinctly significant radiometric response in both the potassium thorium and uranium maps is to the extreme south west (around Ibillo - Ikiran road; Figure 4), which records high concentration of K Th and U and is associated with the granite gneiss in the area. The relics of weathered metasedimentary units which are represented by thin soil cover are identified by the significant Th signature at the north-central of the ternary image.

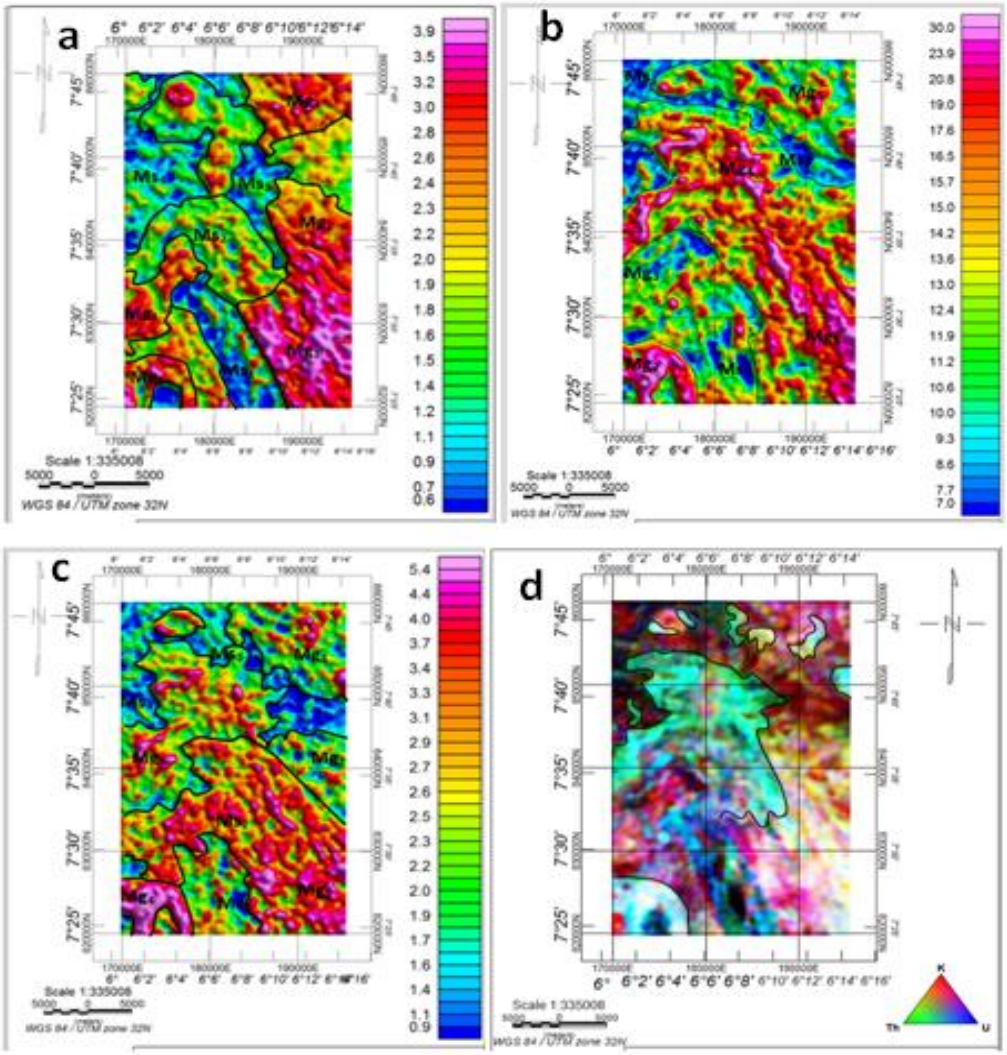

Figure 4: Structural and lithological disposition of the study area viewed from radiometric images: (a) Airborne K (%) image map (b) Airborne eTh (ppm) image map (c) Airborne eU (ppm) image map (d) Airborne ternary composite image map of the study area.

4.3. Lithology and Structures

Field and petrographic studies showed that migmatitic gneiss, biotite schist, quartz schist, granite gneiss, calc-silicate /marble are the main rock types in the study area. Migmatites are essentially metatexites which, to the northwest are dialational, in the northeast they are dialational net-structured and in the southeast straumatic. Quartz, plagioclase feldspar, microcline, muscovite and biotite are the essential minerals in the rocks, while metallic ore minerals identified in the rocks are pyrite, chalcopyrite and magnetite. Biotite-schist is highly migmatized and granitized which results in the rarity of fresh outcrop; where found, it exhibits both mineralogical and lithological banding attributable to a combination of sedimentary fabric S_0 and a subsequent metamorphic fabric S_1. Calc-silicate gneiss, on the

other hand, is characterized by clear, coarse banding which shows alternating white, dark-green and black layers. White layers are predominantly made up of calcite, while dark-green ones are made up of tremolite-actinolite; black layers are made up of biotite and hornblende. The calc-silicate gneiss is associated with dolomitic marble in the southwestern part of Lampese while fragments of calcitic marble, exposed from hand-dug well by residents of Ogale, reflect an entirely different composition. Absence of metaconglomerate may be attributable to two possibilities of either a plunge of folded metasedimentary units which results in increase in the thickness of overburden and hence deeper burial, or a thinning-out, characteristic of sedimentary unit.

Quartz-schist form low-lying outcrops and prominent ridges, resulting in impressive topographic expression. It consists of schistose (flaggy and fissile) and massive varieties. Weathering of the metasedimentary units resulted in the formation of soil cover used for settlement and agriculture, on the migmatite gneisses which are the oldest rocks. Three episodes of deformation D_1, D_2 and D_3 are recognized in the study area. D_1 is attributed to an episode of ductile deformation preserved in the relics of early gneiss. D_2 is associated with that which produced planes of foliations of the main phase gneisses as well as the metasediments while D_3 is interpreted as that which modified the earlier D_1 and D_2; most of the tectonic interpretation of deformational phases is done from the underlying and adjoining gneisses as the metasedimentary units are largely devoid of many structural features due to their location at the periphery of the basin which also results in the weathering and thinning-out of some metasedimentary units like the metaconglomerate.

Figure 6 shows an equal area projection rose diagram (azimuth-frequency-length) for lineaments delineated from aeromagnetic maps showing frequency and length of observed lineament strike direction, in 10 classes. Lineaments delineated on the imagery depict trends in the NE-SW, NW-SE, a few in the E-W, and none in the N-S directions. The rose petals in the NE-SW and NW-SE represent the main strike directions in the region. Figure 6 indicates that out of 44 azimuths values plotted, 40% each represented the two largest petal which strikes 40^0-90^0 (NE-SW) and 280^0 – 345^0 (NW-SE) respectively and which corresponds to the main regional structures of the area. About 10% of the total azimuth values range between 270^0 and 280^0 (E-W) strike which represent minor regional strike of the lineaments. None of the azimuths have values within 0^0-10^0 and 350^0-360^0 (N-S).

Based on the computed lineament density (Figs. 5c&d), areas underlain by migmatite are those with the highest density of lineament followed by areas underlain by metasedimentary rocks. Density of lineaments is generally low in areas underlain by biotite schist and granite gneiss. These areas of relatively high lineament density is shown by the 3D- wire mesh to correspond to the west and southeast of the study area, illustrating a peak corresponding to the migmatite/gneiss terrains while depressions correspond to areas underlain by the metasedimentary units. The high lineament density in the migmatite is probably due to their higher metamorphic grade, which results in a correspondingly higher resistance to weathering, as against the metasediments. Interpretation of magnetic and radiometric data as well as field check confirmed a NW-SE trending fault plane which is believed to be a late, breaking stage of a progressive, regional deformational episode. This fault could serve as conduit for migration of metal-laden hydrothermal fluids that could eventually results in mineral deposition.

Both geophysical and field data give a general configuration of the lithological and structural disposition of the study area. Figure 4 b & d in particular emphasized the NW-SE trending fault. Movement is interpreted to be strike-slip in the northwest direction where it is seen to squeeze the thin layer of weathered metasediments against migmatitic gneisses to the west of the study area; this squeeze, when viewed on digital image, appear in shape like a volcanic lava flow. Orientation of dominant foliation planes of NW-SE and NE-SW in the southeast and southwest respectively of the study area gives an outline of the two opposite limbs of a fold structure that outline the northern closure of the ancient sedimentary basin (Fig. 7); late-stage, brittle-ductile deformation resulted in the compression of this fold structure and subsequent faulting in one of the limbs. Another interesting observation is that majority the measured foliation planes deep gently to the west (Fig. 7 & Table 2).

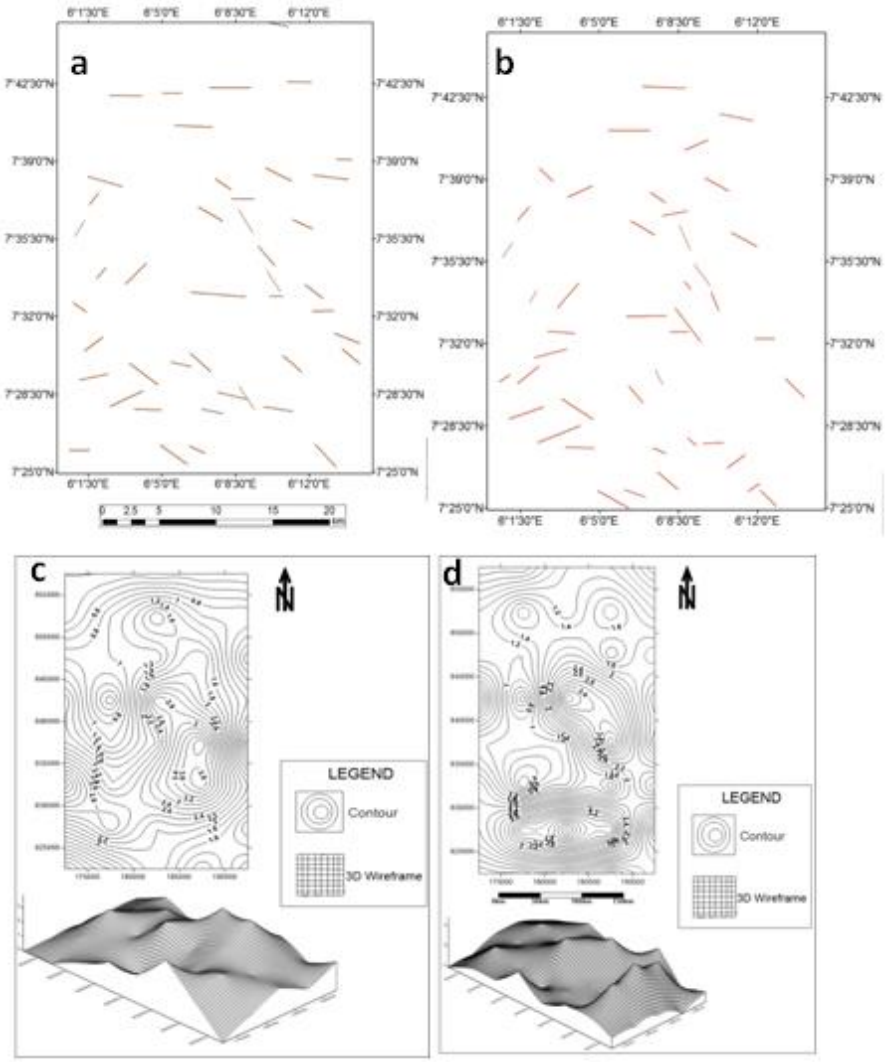

Figure 5: (a) Lineament derived from air borne magnetic data for the study area, (b) Lineament derived from airborne radiometric data, (c) Lineament density contour map for air borne magnetic data (d) Lineament density contour map for air borne radiometric data.

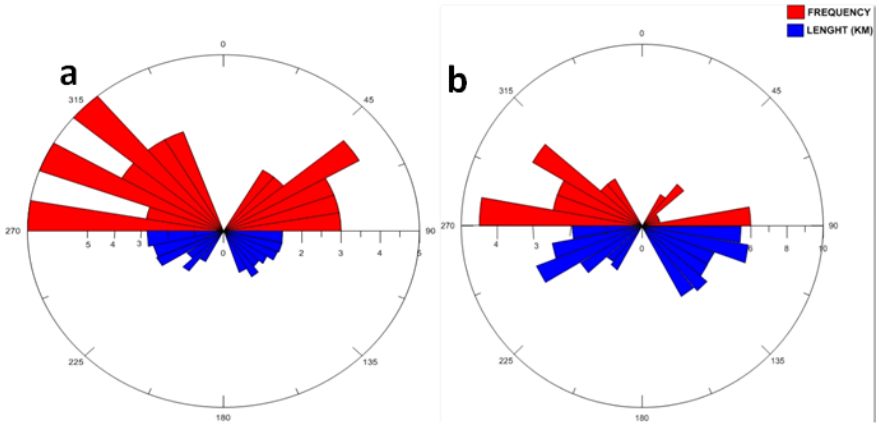

Figure 6: (a) Rose diagram showing length and frequency of lineament from air borne magnetic data for the study area (b) Rose diagram showing length and frequency of lineament from air borne radiometric data for the study area.

Table 2: Measured attitudes of foliation planes from field.

S/N	Azimuth (º)	Dip	Dip Direction	S/N	Azimuth (º)	Dip	Dip Direction	S/N	Azimuth (º)	Dip	Dip Direction
1	350	30	W	**35**	344	50	W	**69**	339	55	W
2	359	41	W	**36**	338	49	W	**70**	300	55	W
3	320	30	W	**37**	340	44	W	**71**	40	60	W
4	340	25	W	**38**	352	32	W	**72**	10	55	E
5	330	32	E	**39**	342	30	W	**73**	6	70	E
6	40	38	W	**40**	323	60	W	**74**	26	42	E
7	310	40	W	**41**	350	49	W	**75**	350	40	E
8	300	60	E	**42**	340	60	E	**76**	80	50	W
9	350	56	E	**43**	335	70	W	**77**	342	40	W
10	350	50	W	**44**	320	68	W	**78**	354	41	E
11	340	40	W	**45**	335	70	W	**79**	354	54	E
12	50	40	E	**46**	336	65	W	**80**	354	52	W
13	340	20	W	**47**	340	60	W	**81**	325	55	W
14	340	36	W	**48**	330	60	W	**82**	344	46	W
15	355	30	W	**49**	69	45	W	**83**	320	57	W
16	350	30	W	**50**	345	35	W	**84**	350	44	W
17	20	33	W	**51**	325	60	W	**85**	13	56	W
18	16	25	W	**52**	335	60	W	**86**	350	54	W
19	0	25	W	**53**	290	43	E	**87**	345	40	W
20	344	41	W	**54**	302	42	E	**88**	335	70	W
21	339	41	W	**55**	323	60	W	**89**	330	88	W
22	345	29	W	**56**	340	60	W	**90**	355	45	W
23	20	31	W	**57**	20	70	W	**91**	05	65	W
24	49	54	W	**58**	310	70	E	**92**	355	87	W
25	49	71	W	**59**	340	40	E	**93**	330	60	W
26	40	52	W	**60**	10	55	W	**94**	345	35	W
27	12	40	W	**61**	340	88	W	**95**	325	80	W
28	20	29	E	**62**	310	50	W	**96**	348	60	W
29	336	35	W	**63**	315	50	E	**97**	350	40	W
30	340	28	W	**64**	328	40	W	**98**	340	75	W
31	21	60	E	**65**	30	40	W	**99**	333	70	W
32	12	40	W	**66**	355	87	W	**100**	345	40	W
33	340	24	W	**67**	355	65	W	**101**	334	74	W
34	342	38	W	**68**	340	75	W				

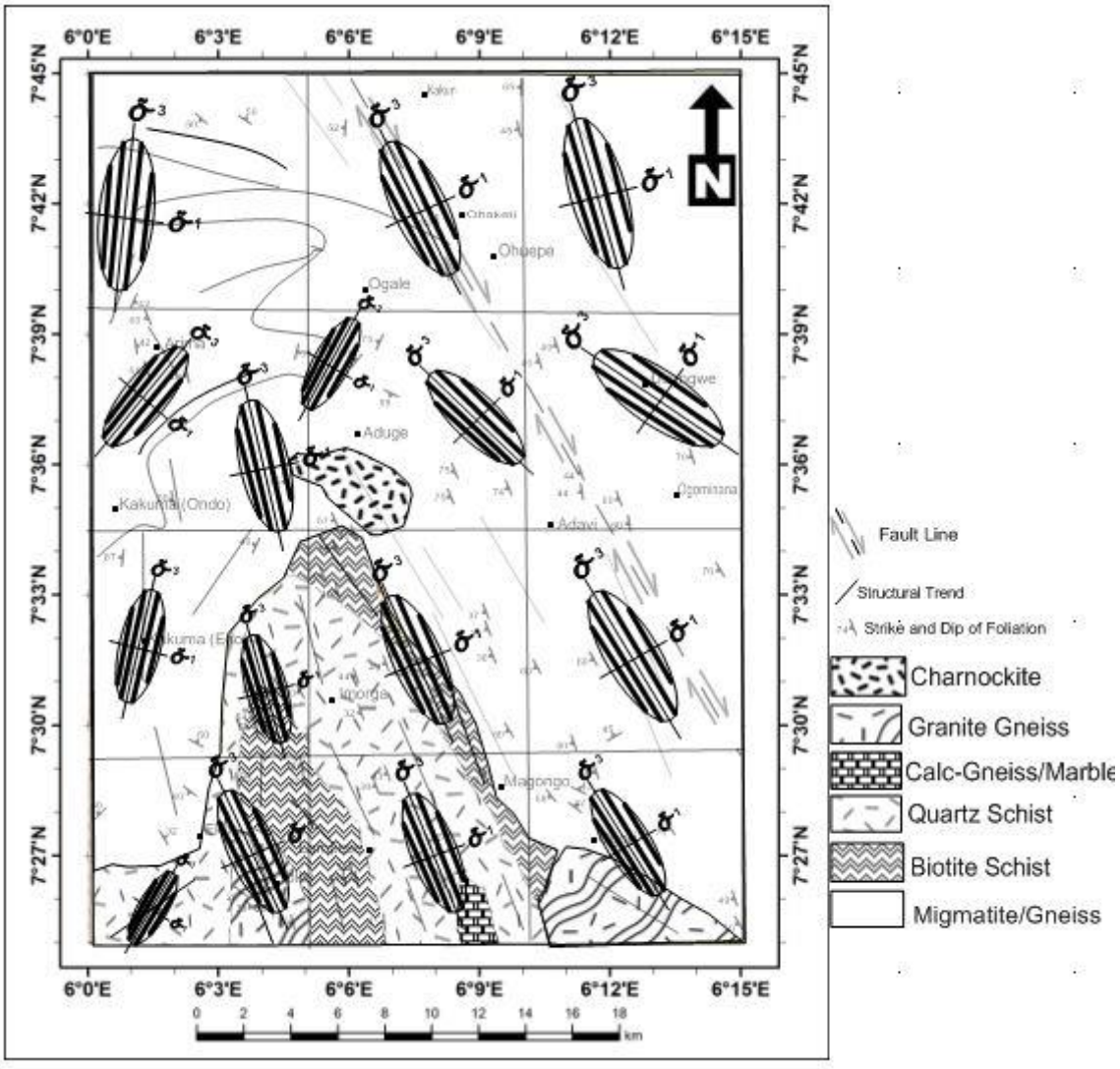

Figure 7: Structural map showing resolved planes of foliation of the entire study area.

5. Conclusion

Integrated geophysical and geological data have helped in delineating lithological boundaries as well as structural architecture of the study area. Discrepancies in the lithological boundaries delineation between magnetic, radiometric and field data are due to differences in response of individual rock units in terms of geophysical parameters. A slight variation in the signature may have occurred where a rock unit at two locations is having one exposed and the other covered by superficial sedimentary materials. The E-W trending lineations are interpreted to partly represent earliest episode of deformation which is retained in the relics of early gneisses which predate the main phase gneisses and the metasediments. The second episode of deformation is believed to have acted in a compressive manner, contributing to

narrowing of the northern part of the metasedimentary basin; the late stage brittle deformation phase of this resulted in faulting in southeast limb of the compressed basin. A third episode of deformation, assumed to be associated with Pan-African orogenic event, is seen to have modification effects on the earlier two. These modifications included axial plane crenulation on the limbs of local folds as well as ptygmatically-folded quartzo-feldspathic veins. Fractures which are essentially in oblique angles to the direction of foliation are believed to be in response to different deformational episodes.

Three deformational episodes identified in the course of this research goes to show that rocks in the present study area have undergone multiple cycles of deformation which is capable of predisposing them to hosting economic mineral deposits, just like their counterparts elsewhere. Faults are known to constitute conduit for ore-bearing hydrothermal fluids which eventually get precipitated along their paths. Lineament length and frequency in the NW-SE direction emphasizes a fault plane, in the present study area, which is a potential pathway for migration of hydrothermal fluids which are in turn key to mineral deposition. This fault, reported in the present study area, could not possibly be an exception in terms of potential for hosting mineralization as indeed gold mineralization reported in Dagbala-Atte area is believed to be associated with this fault in that area which is now found to have extended to the present study area. Also, this study reported the occurrence of marble in association with the metasedimentary rocks for which their counterparts in the southern parts of the Igarra schist belts are known.

References

Adekoya, J. A. (1999): *Rocks and stones: treasure house for national prosperity*. Inaugural Lecture Series **19**, Federal University of Technology, Akure.

Adepoju, M. O. (2017): *Geological and geochemical Exploration studies of Dagbala-Atte District in Igarra Schist Belt, Southwest Nigeria*. (PhD Thesis, Federal University of Technology, Akure, Nigeria).

Airo, M. L. and Loukola-Ruskeeniemi, K. (2004): Characterization of sulphide deposits by airborne magnetic and gamma-ray responses in eastern Finland. *Ore Geology Reviews.* **24** (1), 67-84.

Ajibade, A. C. and Wright, J. B. (1988): *Structural relationships in the Schist belts of northwestern Nigeria*. In: Oluyide, P.O., *et al*. (Eds.), Precambrian Geology of Nigeria. 103–109, (Published by Geological Survey of Nigeria).

Annor, A. E., Olobaniyi, S. B. and Mucke, A. (1996): A note on the geology of Isanlu area in the Egbe-Isanlu Schist Belt, SW Nigeria. *Journal of Minerals Geology.* **32**(1), 47-51.

Ansari, A. H. and Alamdar, K. (2009): Reduction to the Pole of Magnetic Anomalies Using Analytic Signal. *World Applied Sciences Journal.* **7**, 405-409.

Armstrong, M. and Rodeghiero, A. (2006): Airborne Geophysical Techniques in Aziz. University of Wollongong and the Australasian Institute Mining and Metallurgy. *Coal Operators' Conference.* 113-131.

Boadi, B., Wemegah, D. D. and Preko, K. (2013): Geological and structural interpretation of the Konongo area of the Ashanti gold belt of Ghana from aeromagnetic and radiometric data. *International Research Journal of Geology and Mining (IRJGM).* **3**(3), 124-135.

Dickson, B. L. and Scott, K. M. (1997): Interpretation of aerial gamma ray surveys-adding the geochemical factors. *AGSO Journal of Australian Geology and Geophysics.* **17** (2), 187- 200.

Geosoft Inc. (1996): OASIS Montaj Version 4.0 User Guide. Geosoft Incorporated, Toronto.

Geosoft Inc. (1995): OASIS Montaj Airborne Radiometric Processing System Version 1.0 User's Guide. Geosoft Incorporated, Toronto.

Hockey, R. D., Sacchi, R., de Graaff, W. P. F. H. and Muotoh, E. O. G. (1986): The Geology of Lokoja-Auchi area: explanation of 1:250,000 Sheet 62. *Geological Survey of Nigeria. Bulletin* No. **39**, 71.

Mauring, E. and Kihle, O. (2006): Levelling aerogeophysical data using a moving differential median filter. *Geophysics*. **71**, L5–L11.

Minty, B. R. S. (1998): Multichannel models for the estimation of radon background in airborne gamma-ray spectrometry. *Geophysics*. **63**, 1986–1996.

Minty, B. R. S. and Hovgaard, J. (2002): Reducing noise in gamma-ray spectrometry using spectral component analysis. *Exploration Geophysics*. **33**, 172–176.

Ministry of Mines and Steel Development, (2010): Airborne geophysical digital data dissemination guidelines. *World Bank Assisted sustainable management of Mineral Resources Project.* 22.

Muecke, A. (2005): The Nigerian manganese-rich iron-formation and their host rocks from sedimentation to metamorphism. *Journal of African Earth Sciences*. **41**, 407-436.

Murphy B. S. (2007). Airborne geophysics and the Indian scenario. *Journal of Indian Geophysics Union*. **11** (1), 1-28.

Odeyemi, I. B., Olorunniwo, M. A. and Folami, S. I. (1997): Late-proterozoic metaconglomerates in the schist belt of Nigeria: origin and techonostratigraphic significance revisited. *Journal of Technoscience*. **1**(3), 48-55.

Odeyemi, I. B. (1990): The petrology of a Pan-African pluton in Igarra, southwestern Nigeria. *Nigerian Journal of Science.* **28** (2), 181-193.

Odeyemi, I. B. (1988): *Lithostratigraphy and structural relationships of the Upper Precambrian Metasediments in Igarra area, southwestern Nigeria*. In: Oluyide, P. O., W. C. Mbonu, A. E. Ogezi, I. G. Egbuniwe, A. C. Ajibade, and A. C. Umeji. (editors), Precambrian geology of Nigeria. Published by Nigerian Geological Survey Agency. 111 – 125.

Olobaniyi, S. B. and Annor, A. E. (1997): The occurrence of Komatiitic Ultramafic schist in the Egbe-Isanlu schist belt, SW Nigeria and its age implications. Abstract: Nigerian Minerals and Geological Society. 33rd Annual Conference, Jos 97, 12-13.

Patra, I., Chaturvedi, A. K., Srivastava, P. K. and Ramayya, M. S. (2013): Integrated Interpretation of Satellite Imagery, Aeromagnetic, Aeroradiometric and Ground Exploration Data-sets to Delineate Favorable Target Zones for Unconformity Related Uranium Mineralization, Khariar Basin. Central India. *Journal Geological Society of India*. **81**, 299-308.

Reynolds, R. L., Rosenbaum, J. G., Hudson, M. R. and Fishman, N. S. (1990): *Rock*

magnetism, the distribution of magnetic minerals in the Earth's crust, and aeromagnetic anomalies. In Hanna, W.F., ed., Geologic Applications of Modern Aeromagnetic Surveys: United State Geological Survey Bulletin. **1924**, 24-45.

Richardson, K. A. (1983): *Airborne gamma-ray spectrometric survey of the NEA/IAEA Athabasca Test Area, in Uranium Exploration in Athabasca Basin, Saskatchewan, Canada*. In: E.M. Cameron (Ed.), Geological Survey of Canada. Paper 82-11, 1-14.

Schwarz, G. F., Klingele, E. E. and Rybach, L. (1992): How to handle rugged topography in airborne gamma-ray spectrometry surveys. *First Break.* **10**, 11–17.

Shives, R. B. K., Wasyliuk, K. and Zaluski, G. (2000): Detection of K enrichment, illite chimneys using ground gamma ray spectrometry, McArthur River area, northern Saskatchewan, in Summary of Investigations 2000, v.2: *Saskatchewan Geological Survey, Saskatoon. Energy Mines, Miscellaneous Report.* 2000-4.2, 160-169.

Silva, A. M., Pires, A. C. B., Mccafferty, A., de Moraes, R. A. V. and Xia, H. (2003): Application of Airborne Geophysical Data to Mineral Exploration in the Uneven Exposed Terrains of the Rio Das Velhas Greenstone Belt. *Revista Brasileira de Geociências*. **33**, 17-28.

Telford, W. M., Geldart, L. P. and Sheriff, R. E. (1990): *Applied Geophysics*. 2nd Ed. Cambridge University Press, UK.

Turner, D. C. (1983): *Upper Proterozoic Belts in the Nigerian Sector of the Pan-African Province of West Africa*. Precambrian Research (Elsevier Science Publishers), **21**, 55-79.

Udinmwen, E., Oden, M. I. and Danbatta, U. A. (2016). Strain conditions tracked by metamorphic spots in the Igarra schist belt, southwestern Nigeria. *Season of Rahaman, Book of Abstracts for Professionals Symposium*, 14.

Wemegah, D. D., Preko, K., Noye, R. M., Boadi, B., Menyeh, A., Danuor, S. K. and Amenyoh, T. (2015): Geophysical Interpretation of Possible Gold Mineralization Zones in Kyerano, South-Western Ghana Using Aeromagnetic and Radiometric Datasets. *Journal of Geoscience and Environment Protection*. 2015, **3**(4), *67-82.*

Wilford, J. R., Bierwirth, P. N. and Craig, M. A. (1997): Application of airborne gamma-ray spectrometry in soil/regolith mapping and applied geomorphology. *Journal of Australian Geology and Geophysics.* **17**(2), 201–216.

Wilford, J. (2002): *Airborne gamma-ray spectrometry. Cooperative Research Centre for Landscape Envirionments and Mineral Exploration*. Commonwealth Scientific and Indusctrial Research Organization, Bertley, WA, Australia. Open File Rep. 144, 46-52.

Wright, J. B., Hastings, D. A., Jones, W. B. and Williams, H. R. (1985): *Geology and Mineral Resources of West Africa.* George Allen (Boston) & Unwin (Sydney), London.